Materials Advances

ROYAL SOCIETY OF CHEMISTRY

PAPER

View Article Online
View Journal | View Issue



Cite this: *Mater. Adv.*, 2025, **6**, 1031

# Investigation of the mechanical properties of an aluminum (Al 6061-T6)/graphene/bentonite hybrid nanocomposite experimentally and through finite element analysis study

Hasan Bawa'neh, Bashar Lababneh, Ahmad M. Malkawi and Ayat Bozeya *

Nanoparticles are a useful addition to existing materials as they enable the development and production of nanocomposites with enhanced properties. Hybrid nanocomposites with more than one nano–reinforcement material provide the ability to further enhance the properties of the nanocomposite. This research is focused on fabricating a hybrid nanocomposite containing graphene sheets and nanoclay in an aluminum alloy metal matrix (Al 6061-T6). Sandcasting technique was used to prepare the nanocomposite using templates fabricated using 3D printers (FDM) and 3D models. The ductility of the aluminum alloy helps with stress distribution throughout the matrix phase onto the reinforcement nanoparticles and nanosheets, which causes a significant improvement in the mechanical properties of the nanocomposite. Fourier transform infrared (FTIR) spectroscopy and scanning electronic microscopy (SEM) imaging were used to characterize the materials, along with universal standard mechanical tests. Computer aided tests were also performed using COMSOL software, and the results matched, showing the enhancement of the properties of the composite. Anti-microbial behavior of the nanoclay was tested, which showed an inhibition zone around the 2% nanoclay in disk diffusion test. Thus, an innovative nanocomposite material was developed by integrating graphene and nanoclay into Al 6061-T6. This combination not only enhances mechanical properties—such as deformation resistance and tensile strength—but also introduces antimicrobial activity on the aluminum surface. The improved properties make this nanocomposite particularly suitable for high-touch applications where both durability and hygiene are crucial, including doorknobs, toilet flushes, and shopping carts.

Received 4th September 2024,
Accepted 9th December 2024

DOI: 10.1039/d4ma00890a

rsc.li/materials-advances



## 1. Introduction

A combination of two distinct materials in two distinct phases, a continuous matrix and discontinuous particulate reinforcement phase, is called a composite.[1] Nanocomposites (NCs) have been of great interest and have grabbed the attention of many researchers owing to their enhanced properties over larger size particles. Particles are considered within the nanoscale when their dimensions are in the range of 1–100 nm.[2,3] Hybrid composites is a term that refers to matrices containing more than one reinforcement material.[4] Hybrid composites offer the benefit of filler material properties being enhanced by other filler materials.[5] Hence, nanocomposites can be prepared in multiple combinations of materials and characterized into three basic building blocks depending on the matrix material, *i.e.*, ceramics, polymers, and metals.[3,6] The resulting materials from nanocomposites can have a combination of drastically different mechanical, chemical, electrical, optical, and thermal properties from the original matrix material.[7–9] Nanoparticles can also split into four main blocks depending on their geometries. Nanoparticles can be zero-dimensional (core shell structure), one dimensional (nanowires and nanotubes structure), two dimensional (lamellar structure) and three-dimensional (metal matrix composite structures).[10] There are many diverse types of nanofillers that can be used, including carbon-based nanomaterials, inorganic and organic-based nanomaterials, and composite-based nanomaterials.[11]

The current research focused on the preparation of hybrid nanocomposite materials by the addition of graphene sheets and nanoclay into an aluminum metal matrix. This combination of graphene, nanoclay, and aluminum enhanced mechanical properties—such as deformation resistance and tensile strength—and introduced antimicrobial activity on the aluminum surface. The hybrid nanocomposite was prepared using the common sandcasting technique.[12–14] Graphene is

*Institute of Nanotechnology, Jordan University of Science and Technology, Irbid, 22110, Jordan. E-mail: aabouzieh@just.edu.jo*

made up of a single layer of packed carbon atoms arranged in a hexagonal honeycomb lattice. It is a plane of $sp^2$-bonded atoms, which makes it an allotrope of carbon. The thickness of a graphene sheet is approximately 0.34 nm, and its size can range from a few nanometers to centimeters, depending on the production process. Graphite-derived materials are fullerene, graphene quantum dots, carbon nanotubes, and graphene nanoribbons. A graphene sheet is necessary for all derivatives. In a graphene sheet, Sigma bonds or covalent bonds between carbon atoms in the same plane, are stronger than bonds or weaker bonds found outside the plane.[15]

Graphene nanosheets are used as nanofillers in different advanced applications such as batteries, super capacitors, and sensors.[16,17] Graphene sheets can transfer stresses efficiently to improve the mechanical properties of the host matrix material due to its large specific surface area. The thermal and dynamic properties of the matrix material can also be improved by adding graphene sheets.[18] Many studies have also reported that graphene sheets result in an increase in stiffness and strength higher than carbon nanotubes and with cheaper cost and more ease in manufacturing.[19,20] Nanoclay is an excellent material for incorporating nanocomposites due to their wide availability, low cost and environmental impact.[21] Nanoclays are layered silicates mineral nanoparticles that can form complex crystallites.[22] There are thirty diverse types of nanoclays each with unique properties, which can be used for different applications.[23] Bentonite is a type of nanoclay that has been used as a drilling fluid additive and can be used as a matrix material or as a nanofiller. As a nanofiller, its main function is to increase plasticity in ceramic bodies.[24] Aluminum matrix can also have a variety of alloys. Precipitation-treated aluminum alloys, such as Al 6061-T6, are some of the most promising options for developing thermally stable, exceptionally durable, and lightweight nanostructured materials. Optimal precipitate distribution in precipitation-treatable alloys (T6 temper) ensures the greatest strength of the material. Therefore, considerable strain deformation of aluminum alloys in the T6 temper is a feasible method to manufacture nanostructured materials with a fine dispersion of precipitates distributed uniformly throughout the matrix.[25,26]

Al 6061-T6 is a heat-treated aluminum alloy renowned for its high strength, lightweight properties, and excellent corrosion resistance. Belonging to the 6xxx series, it is primarily composed of aluminum, magnesium, and silicon, which together create a material with balanced mechanical properties. The ''T6'' designation refers to the specific heat treatment process, which involves solution heat-treating, followed by artificial aging, thus enhancing the alloy's yield and tensile strength.

Al 6061-T6's mechanical properties make it ideal for applications requiring durability and structural integrity, such as aerospace, automotive, marine, and structural components. The alloy is particularly advantageous due to its machinability and ability to undergo welding without significant loss in strength, unlike many other high-strength aluminum alloys. Additionally, it can be easily anodized to improve the surface hardness and corrosion resistance further, making it suitable for both indoor and outdoor applications in high-stress environments.[27]

Aluminum matrix composites (AMCs) are an increasingly valuable class of materials due to their unique blend of high strength-to-weight ratio, enhanced durability, and improved thermal properties, which make them ideal for demanding applications in aerospace, automotive, and defense industries. By embedding various reinforcing particles, such as ceramics or carbon fibers, within the aluminum matrix, AMCs achieve superior mechanical and physical properties over standard aluminum alloys. The development of hybrid aluminum matrix composites (HAMCs), which include multiple types of reinforcements, has further expanded the versatility of AMCs, allowing for tailored properties that meet specific application needs.

Research in this field is critical not only because it enables lighter, stronger materials that can improve the fuel efficiency and reduce emissions but also because it provides insights into cost-effective and scalable manufacturing methods that could make advanced materials more accessible. HAMCs offer vast potential for innovation by allowing control over parameters such as reinforcement type, size, and distribution, which directly affect the composite's strength, wear resistance, and fatigue life. Ongoing studies aim to optimize these properties for industrial use, exploring diverse manufacturing techniques, such as powder metallurgy and stir casting, to fine-tune their performance and make AMCs a cornerstone of next-generation engineering materials.[28]

Incorporating bentonite clay into aluminum composites can enhance the mechanical properties exploiting bentonite's layered structure and high surface area, which allows it to function as a reinforcing agent within the metal matrix. The intercalation of bentonite layers within the aluminum matrix forms a strong interface, which restricts the mobility of aluminum atoms, thereby improving the composite's tensile strength and hardness. Additionally, bentonite's high cation exchange capacity aids in forming robust bonds with aluminum, further contributing to the composite's rigidity and thermal stability.

The addition of bentonite clay also acts as a barrier against crack propagation under stress, which is crucial for applications requiring high durability and strength. When uniformly distributed within the aluminum matrix, bentonite enhances wear resistance and reduces material degradation under cyclic loads. This makes bentonite-reinforced aluminum composites suitable for applications in industries like automotive and aerospace, where lightweight, high-strength materials are essential. Techniques such as powder metallurgy and stir casting can be used to disperse bentonite clay effectively, ensuring even distribution within the aluminum matrix for optimal performance.[29]

There are several uses for metal-matrix nanocomposites (MMCs) with reinforcing materials in the thermal management, automotive, entertainment, defense, aerospace, and infrastructure sectors. High electrical and thermal conductivity, high wear and corrosion resistance, high strength-to-weight ratio, high precipitation strengthening, and high damping

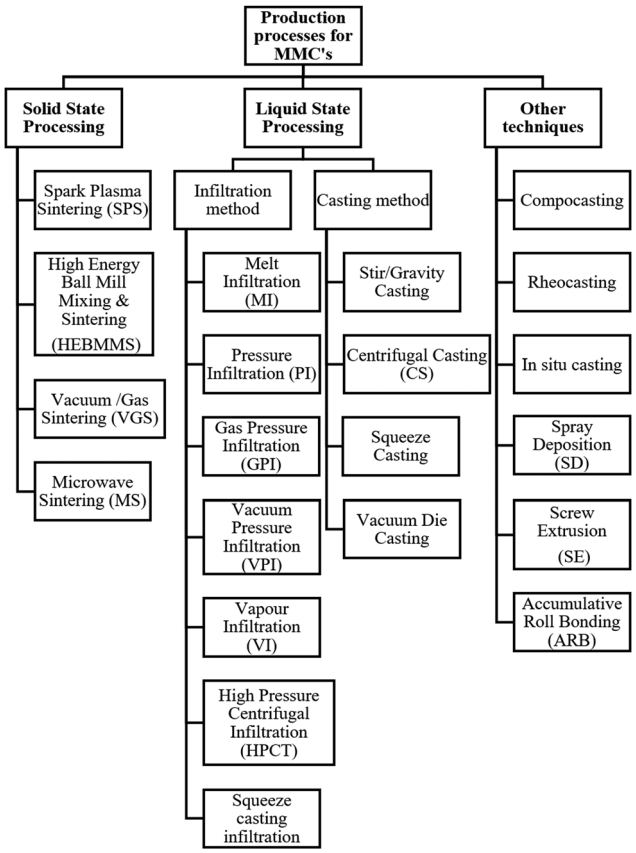


Fig. 1 Processing methods used for MMC fabrication.[33]

capacity are only a few of the characteristics of metal-matrix nanocomposite (MMCs).[30] Several processing procedures were used for fabricating MMCs (Fig. 1), including squeeze casting, gas infiltration, and combo casting, which are all employed in the metal smelting of composite materials. Combo casting is the method of creating a network of MMCs by combining the mixture with whiskers, particles, or short fibers prior to casting.[31,32]

This research focused on creating a hybrid nanocomposite from Al 6061-T6 matrix, which is a malleable metal that can distribute stresses to the filler materials, which will absorb the stresses, hence improving the mechanical properties. The two graphene and bentonite clay nanofiller are chosen as both sheets and particulates to maximize the stress absorption. The nanoclay also demonstrates antimicrobial activity. Tensile, impact, and creep tests were implemented on the hybrid nanocomposite (Alc), and standard molds for these tests were fabricated *via* 3D printing. The sandcasting processing method was used for hybrid nanocomposite fabrication. The SEM images of the nanofillers along with the SEM of the nanocomposite were analyzed. In addition, mechanical tests and antimicrobial tests were also performed.

The improved properties make this nanocomposite particularly suitable for high-touch applications, where both durability and hygiene are crucial, including doorknobs, toilet flushes, and shopping carts. Additionally, the research includes a comprehensive Finite element analysis (FEA) study to simulate and understand the mechanical behavior of the nanocomposite, offering a detailed insight into its potential for widespread use in environments that demand both mechanical robustness and antimicrobial protection. This dual functionality, combining strength with health safety, represents a significant step forward in material design and application.

## 2. Materials and methods

### 2.1 Materials

The following chemicals and materials (Table 1) were used as received.

### 2.2. Methods

The experimental procedure began with the synthesis of graphene using a chemical reduction method, followed by characterization through techniques such as Raman spectroscopy and scanning electron microscopy (SEM) to ensure the quality and structural integrity of the material. The Al 6061-T6 aluminum was then melted, and the synthesized graphene powder, along with nanoclay, was added to the molten aluminum and thoroughly mixed to achieve a homogenous blend. This mixture was introduced into pre-designed molds using the sand-casting technique. The molds were meticulously designed using SOLIDWORKS CAD software and fabricated through fused deposition modeling (FDM) 3D printing to ensure precise dimensions. Once the molten composite was poured into the molds, the casting process was conducted at controlled temperatures to facilitate the proper solidification of the nanocomposite. After solidification, the samples underwent mechanical testing, including tensile and impact tests, to evaluate their enhanced properties compared to the pure Al 6061-T6 samples. Additionally, a finite element analysis (FEA) study was performed using COMSOL Multiphysics software to analyze the mechanical behavior of the nanocomposite, visualizing stress distribution and total deformation under applied loads. This comprehensive methodology effectively demonstrates the fabrication and characterization of the innovative Al 6061-T6/

Table 1 Specification of the materials used

| Material | Specification | Company/Country |
|---|---|---|
| Sulfuric acid | 98 wt% | Sigma Aldrich, Germany |
| Nitric acid | 70 wt% | SDFCL S D Fine Chem Limited, Maharashtra, India |
| HB2 pencils core | Applied in the extraction of graphite | |
| Nanoclay | Hydrophilic bentonite | Sigma-Aldrich-Merck |
| Deionized water | Deionized | Milli-Q water (Direct-Q3 UV) |

Table 2 Experimental parameters for graphene-Al 6061-T6 mechanical testing

| Parameter | Value/description | Unit |
|---|---|---|
| Aluminum alloy | 6061-T6 | |
| Mixing ratio | Graphene to Al6061-T6 | % If applicable |
| Casting technique | Sandcasting | |
| Mold design software | SOLIDWORKS CAD | |
| Mold type | Standard sample sizes and shape for tensile and impact testing | |
| 3D Printing technique | FDM (Fused deposition modeling) | |
| 3D Printing material | Filament used for 3D printing mold | Ex. PLA, ABS |
| Tensile sample size | Specific dimensions used for tensile test molds (ASTM E8) | mm |
| Impact sample size | Specific dimensions used for tensile test molds (ASTM E23) | mm |
| Mold temperature | Temperature during casting process | °C |
| Solidification time | Time needed for materials solidification in the mold | Minutes |

graphene/nanoclay nanocomposite, highlighting its enhanced mechanical properties and antimicrobial activity. All parameters considered during the experiments are summarized in Table 2.

**2.2.1. Graphene sheets' synthesis.** The graphene sheet was prepared using the method described by Vertuccio *et al.* (2019). The method employed by Vertuccio for the preparation of exfoliated graphite involved using natural flake graphite with specific characteristics, including a carbon purity of 98.6% and an average diameter of 500 μm. In his approach, a mixture of nitric and sulfuric acid was utilized for intercalation, which allowed the graphite to expand upon exposure to high temperatures (900 °C), leading to the formation of exfoliated graphite (EG).[34]

In brief, nitric acid and sulfuric acids were combined with natural graphite (volume ratio: 135 mL/255 mL). Intercalation inside graphene sheets occurred after 24 hours of reaction, resulting in intercalated graphite. The mixture was next filtered, washed with deionized water, and dried in a low-heat oven (40 °C), The mixture was then stirred on a magnetic stirrer in a solution of deionized water, followed by 2 hours of ultrasonication. Finally, the sample was thermally annealed at 300 °C.[34]

The current study adapted Vertuccio's method while utilizing pencil core graphite instead of natural flake graphite. The pencil lead was subjected to rigorous stirring on a hot plate at elevated temperatures to facilitate the exfoliation of graphene flakes. In addition to Vertuccio's chemical intercalation, this method also relies on mechanical agitation and thermal energy to achieve exfoliation. After extraction, the graphene flakes were processed, washed multiple times, and annealed to enhance yield and optimize their properties. This adaptation demonstrates a novel approach to graphene production utilizing a readily available and cost-effective source.

**2.2.2. CAD.** According to the test conducted on the hybrid nanocomposite, a different template was designed using CAD. A 3D design was made as shown in Fig. 2 and then they were printed using delta FDM 3D printers.

**2.2.3. Fabrication of the hybrid nanocomposite material.** In the sand-casting process, all synthesized nanomaterials were turned to powder and encapsulated in aluminum foil. 3D printed samples of all the desired shapes were used to create sand molds. Al 6061-T6 was melted in electrical furnace, then

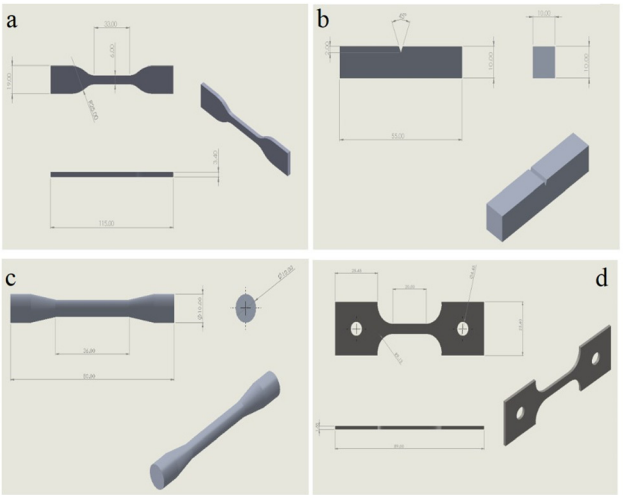


Fig. 2 3D design for the examination samples. (a) CAD model for tensile specimen. (b) CAD model for impact specimen. (c) CAD model for torsion specimen. (d) CAD model for creep specimen.

1 wt% nanoclay and 2 wt% graphene was added to the melted aluminum to create the composite. Proper distribution was necessary for enhanced properties of the composite. Mixing was done *via* a mechanical stir mixer. Fig. 3 summarizes the main steps for the hybrid nanocomposite preparation.

**2.2.4. Simulation.** The simulation part was done using COMSOL software. Tensile test was done using a load force of 1000 N and the thermal stress test was done using 500 N load force at a temperature of 473.15 K. COMSOL Multiphysics was chosen for this research to simulate the tensile strength and deformation behavior of the nanocomposite compared to the pure aluminum sample. The simulation results indicate that the nanocomposite, which integrated the synthesized graphene with Al 6061-T6, demonstrated improved deformation resistance and reduced elongation under the same loading conditions when compared to the aluminum-only sample. While alternative software such as ANSYS and Abaqus also offer robust simulation capabilities, COMSOL's strengths lie in its multiphysics integration and in the ease of handling custom material properties and accurate mesh generation, which made it a suitable choice for capturing the intricate behavior of the graphene-Al 6061-T6 composite. These features facilitated a

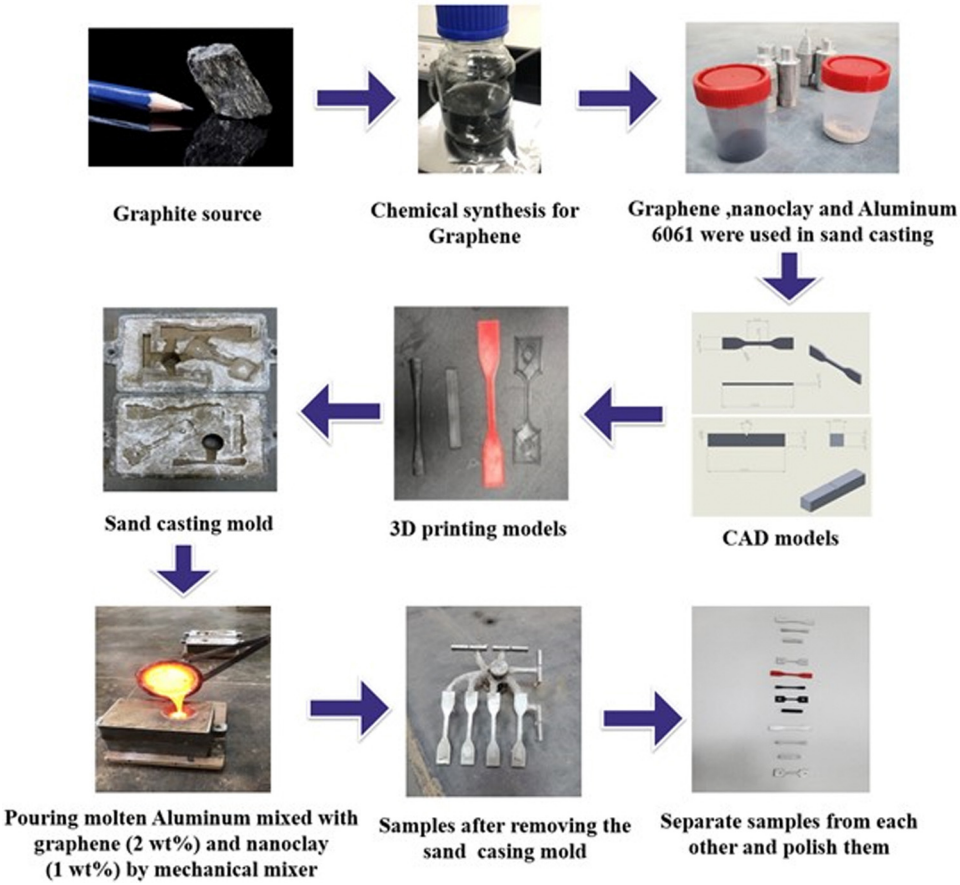


Fig. 3 The main steps for the preparation of the hybrid nanocomposite.

comprehensive analysis of deformation, providing valuable insights into the material's enhanced mechanical properties.

## 3. Results and discussion

### 3.1. Graphene characterization

Fig. 4 shows the SEM images of the prepared graphene sheets. As shown from the SEM images, the obtained graphene flakes had a size of approximately 2 ± 3 μm with some flakes and a dimension of 6 × 6 μm.

Fig. 5 shows the FTIR spectra of the prepared graphene. The spectra show different types of oxygen functionalities peaks, which has a good agreement with previous work.[34] The OH groups peak appeared at 3203 $cm^{-1}$, which indicate that the sample contained water. The two peaks at 2923 $cm^{-1}$ and 2851 $cm^{-1}$ are assigned to the C–H ($sp^3$) bonding because the sample was prepared in acidic media, which indicates the presence of carboxylic acid in the structure. The peak at 1614 $cm^{-1}$ is assigned for the C═C group. The peak at 1706 $cm^{-1}$, 1236 $cm^{-1}$ and 1038 $cm^{-1}$ are assigned to the C═O and C–O of the carbonyl groups.

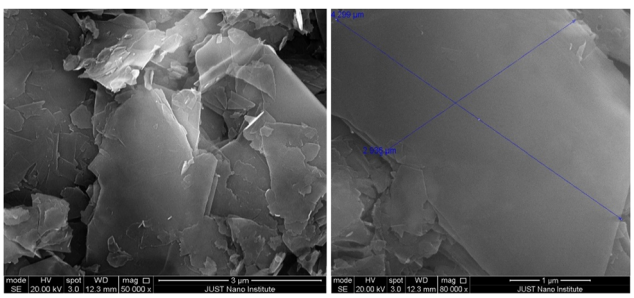

Fig. 4 SEM images of the prepared graphene sheets.

### 3.2. Bentonite nanoclay characterization

The FTIR spectra of bentonite clay are shown in Fig. 6. The spectra show the presence of the OH group peaks at 3612 $cm^{-1}$ and 3434 $cm^{-1}$, which are related to the free and/or combined OH group. The peak at 1634 $cm^{-1}$, which corresponds to the H–O–H angular deformation, confirmed the presence of $H_2O$. The peak at 1002 $cm^{-1}$ is for the asymmetric Si–O stretching, the peak at 516 $cm^{-1}$ is for the Si–O vibration, and the peak at 433 $cm^{-1}$ is for the O–Al vibration. The peaks at 1002 $cm^{-1}$, 433 $cm^{-1}$ and 516 $cm^{-1}$ confirmed the structure of the bentonite nanoclay, which has a good agreement with previous work.[35,36]

### 3.3. Nanoclay antimicrobial test

A zone of inhibition test, often referred to as the Kirby–Bauer test, antimicrobial susceptibility test, disk diffusion test, or

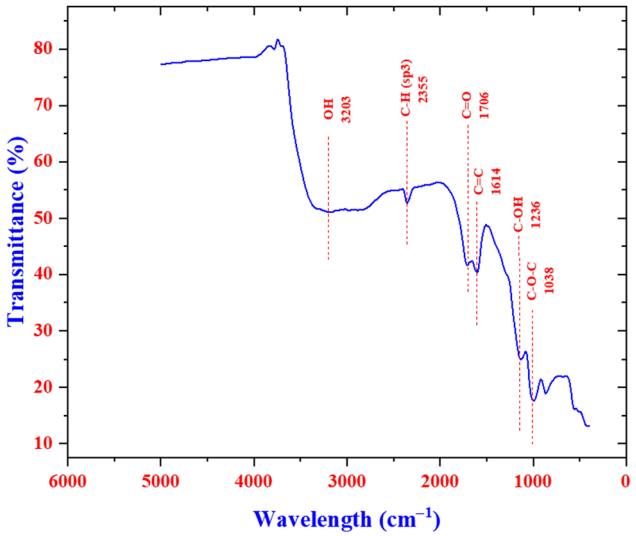


Fig. 5 FTIR spectra of graphene.

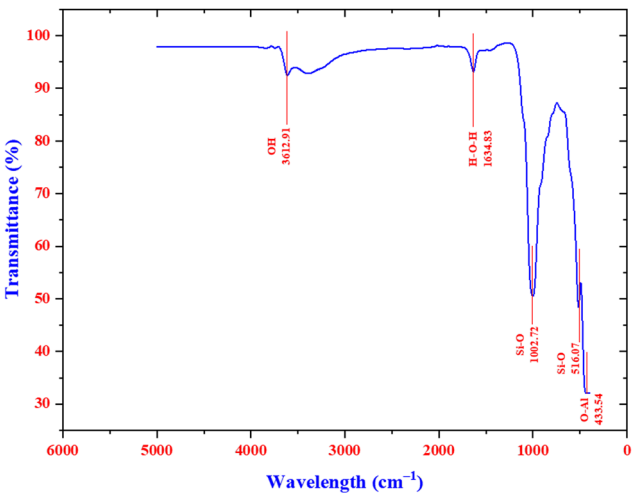


Fig. 6 FTIR spectra of bentonite nanoclay.

agar diffusion test, is an efficient method for determining the antimicrobial activity of a substance or solution with respect to a particular target bacterium. Two types of bacteria were used (*E. coli* and *Staphylococcus aureus*) with 0.1 concentration. Bentonite solutions with 1%, 2% and 3% concentration were mixed and assessed for their antimicrobial activity. The solution with 2% concentration showed the best effects after 24 h, creating a zone around it. Fig. 7 shows the antimicrobial activity of bentonite nanoclay.[29]

The zone of inhibition was not large due to the solution being evaporated, quickly leaving the nanoclay behind and not showing any diffusion. Nevertheless, a 5 mm zone of inhibition was observed along with the prohibition of bacteria growth on the wells of the sample. This indicates that bentonite nanoclay has antimicrobial activity.

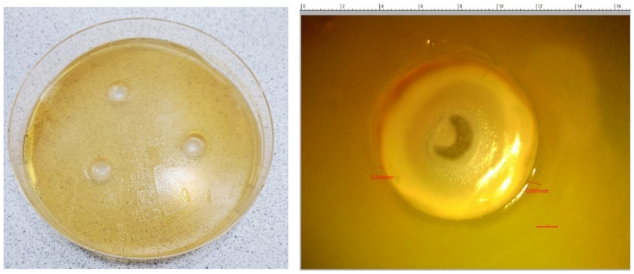

Fig. 7 Antimicrobial behavior of bentonite nanoclay with 2% concentration.

### 3.4. Hybrid nanocomposite characterization

Fig. 8 shows the SEM images for the pure Al 6061-T6 matrix and the hybrid nanocomposite. As shown in the figure, Al (Fig. 8a) has a layer shape. Fig. 8b shows a homogeneous distribution of the nanofiller in the Al metal matrix. Both the graphene sheets and the nanoclay were homogeneously distributed as an aggregate in the Al matrix.

### 3.5. Impact test

The energy absorption of the material is considered as an indicator of the material capacity to withstand sudden applied load without fracturing. This parameter is crucial to evaluate the material resistance to dynamic stresses.[37]

The effect of the nanofillers on the impact strength of the Al 6061-T6 hybrid nanocomposite is shown in Fig. 9. The Charpy v-notch test was performed, the test was repeated four times, and the test sample (prepared according to ASTM E23) had dimensions of 5.5 cm in length and 1 cm square width and height. The addition of the hybrid nanofiller to the Al matrix decreased the impact strength by 52.3% (the average absorbed energy by pure Al was 8.13 N m, while the average absorbed energy by the hybrid nanocomposite was 3.88 N m). The addition of nanoclay and graphene in Al 6061-T6 reduces the plastic deformation energy for the hybrid nanocomposite, which increases the chance of detachment during the fracture, which leads to improved hardness of the more brittle material. Comparable results were reported by Samal and Vundavilli.[38]

According to research, the amount of graphene in graphene/Al composites has a major impact on their mechanical properties. Significant improvements in the mechanical

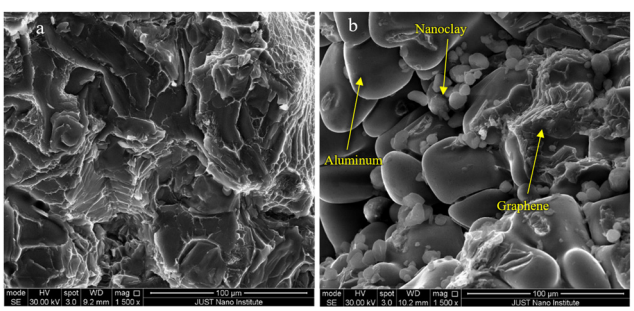


Fig. 8 (a) SEM image of pure Al. (b) SEM image of the nanocomposite.

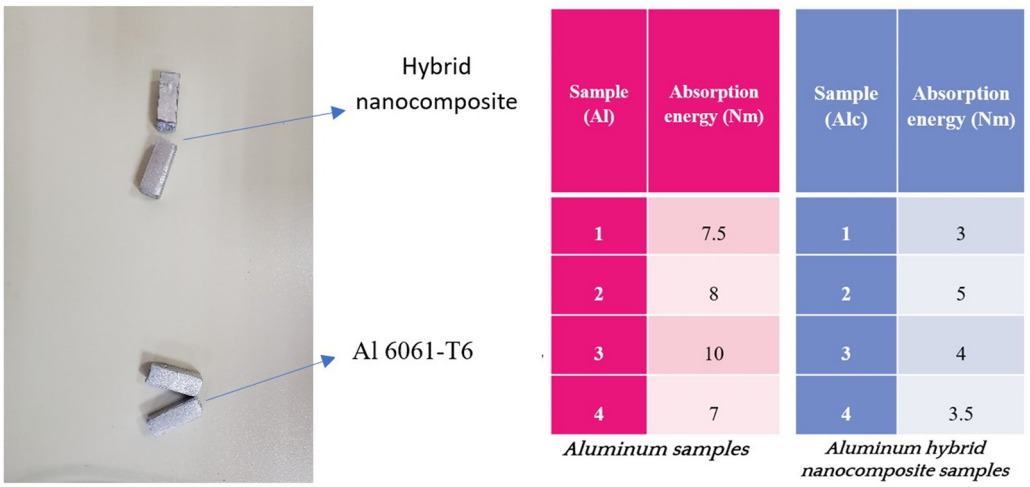


| Sample (Al) | Absorption energy (Nm) |
|---|---|
| 1 | 7.5 |
| 2 | 8 |
| 3 | 10 |
| 4 | 7 |

*Aluminum samples*

| Sample (Alc) | Absorption energy (Nm) |
|---|---|
| 1 | 3 |
| 2 | 5 |
| 3 | 4 |
| 4 | 3.5 |

*Aluminum hybrid nanocomposite samples*

Fig. 9 Impact test results for the pure Al 6061-T6 matrix and the hybrid nanocomposite.

characteristics are often the result of a strong interfacial contact between graphene and the aluminum matrix when graphene is present in trace levels (*e.g.*, 0.5 w/%). These improvements are ascribed to graphene's uniform distribution, which improves the load-bearing capability and prevents dislocation movement.[39]

### 3.6. Tensile test

The tensile test was performed using a universal tensile testing machine (ASTM E8/E8M) in triplicate for each sample. Samples of pure Al 6061-T6 matrix and the hybrid nanocomposite material were prepared in a dog bone shape according to the ASTM E8 standard test. As shown in the stress strain curves in Fig. 10, an increase in the tensile strength in the nanocomposite compared to pure Al can be observed. The ultimate tensile strength for pure Al was 130.6 Mpa compared to 146.77 Mpa for the nanocomposite with up to 118% improvement, which indicates that the addition of graphene sheets and bentonite nanoclay has a positive effect and enhances the mechanical properties of the hybrid nanocomposite.

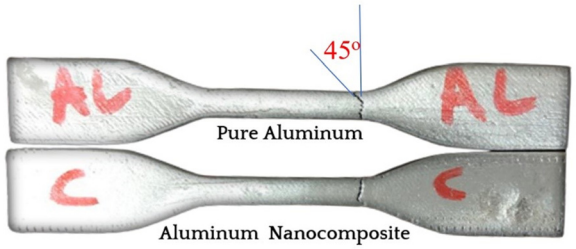


Fig. 11 Hybrid nanocomposite and pure Al fractures after the tensile test.

Fig. 11 shows different fracture shape for the pure Al sample and the Al-Nanocomposite sample after the tensile test, where the nanocomposite has less than 45° fracture and pure Al has almost 45° fracture, which indicates that the nanocomposite has more tensile strength.

### 3.7. Finite element analysis

**3.7.1. Tensile simulation.** Engineering uses the theoretical idea of von Mises stress to predict if a material may fracture or

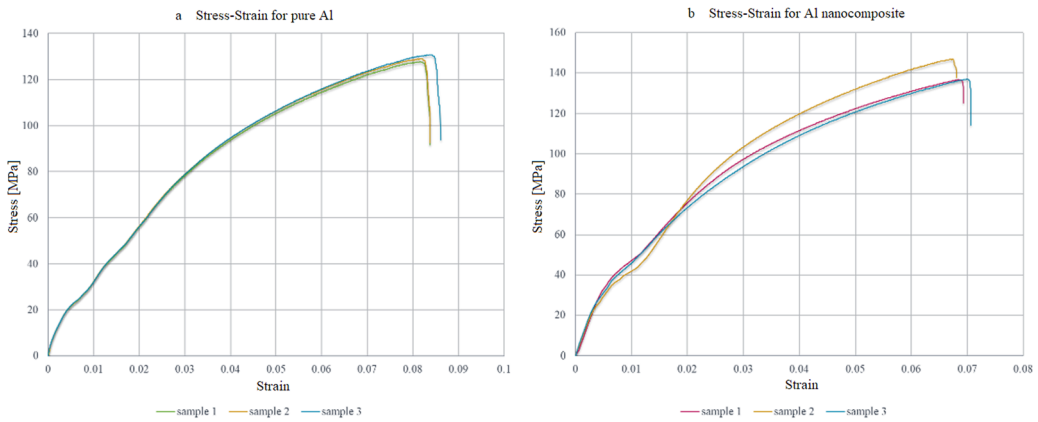


Fig. 10 Stress strain curves for pure Al (a) and the hybrid nanocomposite (b).

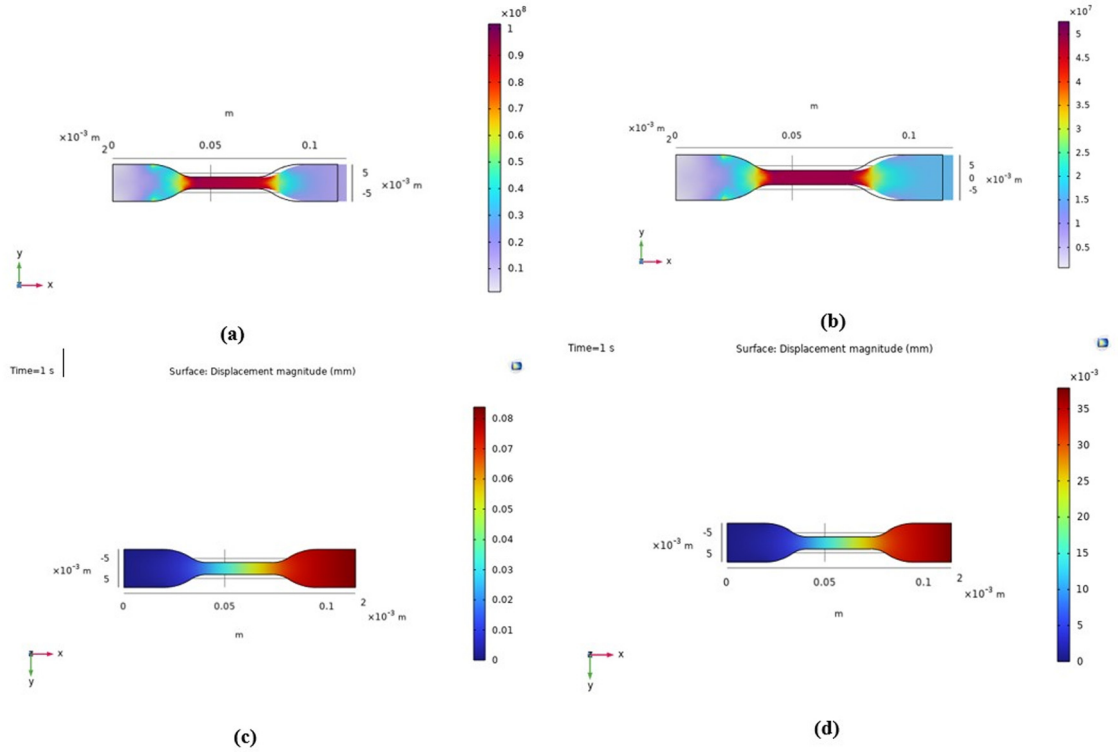


Fig. 12 Stress distribution in (a) the Al and (b) nanocomposite samples, and total deformation in (c) the Al and (d) nanocomposite samples.

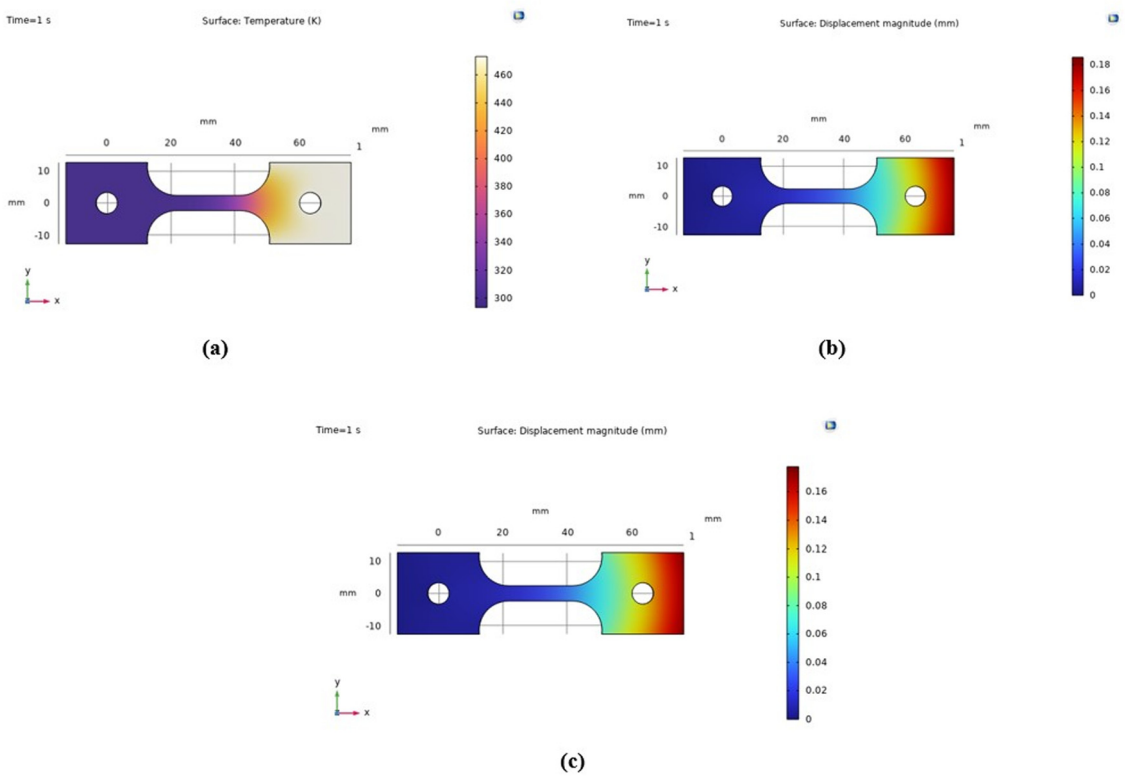


Fig. 13 Temperature distribution (a) and resultant total deformation in (b) the Al and (c) hybrid nanocomposite samples.

yield under complicated loading conditions. It is based on the principle of distortion energy and aids in determining how a material will react to many axial stress conditions.[40]

A three-dimensional multiscale finite element (FE) representative volumetric element (RVE) has been created to examine the mechanical behavior of aluminum graphene nanocomposite (AGNC). A thorough evaluation of the impact various graphene nanoplatelets (GNP) weight fractions, sizes, and orientations on the overall mechanical characteristics is made possible by this modeling technique. FE analysis improves our understanding of how GNP reinforcement may be tuned in aluminum matrices by providing light on the nanoscale stress distribution and deformation mechanisms.[41]

A simulation was made to evaluate the tensile strength and note the change in deformation as the nanocomposite sample showed an improvement in the deformation resistance, and the elongation values were lower compared to the aluminum sample (Fig. 12a–d), where the same load was applied to both the aluminum sample and the nanocomposite sample.

**3.7.2. Thermal stress simulation.** A low tensile force was applied in addition to a temperature difference on both sides to observe the deformation in the sample (Fig. 13a–c).

From the simulation data, it was observed that the amount of total deformation in the nanocomposite sample is less than that in the aluminum sample.

## 4. Conclusion

This research showed the fabrication and characterization of a hybrid metal matrix nanocomposite using aluminum alloy matrix with graphene sheets and bentonite nanoclay as reinforcement materials and how the results match the computer-generated tests. Different tests show the quality of the synthesis materials. Graphene sheets synthesized had an average size of 3 × 3 μm. Also, the resulting nanocomposite showed exceptional mechanical behavior. Tensile test results were as expected and showed a 118% improvement in tensile strength. These results show how the ductility of the aluminum alloy helps distribute the stresses along the nanoparticles used that have high stiffness and strength. Antimicrobial tests also show the effectivity of bentonite nanoclay in the antimicrobial behavior. This composite with enhanced properties can have a variety of different applications at the industrial level. The improved properties make this nanocomposite particularly suitable for high-touch applications where both durability and hygiene are crucial, including doorknobs, toilet flushes, and shopping carts. In summary, the incorporation of graphene sheets and bentonite nanoclay into an aluminum matrix has been shown to enhance its mechanical properties and antimicrobial effect. This dual functionality, combining strength with health safety, represents a significant step forward in material design and application. This research presents an interesting approach towards developing materials with improved properties for various applications, such as in the automotive industry, aerospace industry, and structural materials. Further research and development are required to optimize the processing, characterization, and performance of the proposed composite.

## List of abbreviation

| | |
|---|---|
| Alc | Aluminum hybrid nanocomposite |
| AGNC | Aluminum graphene nanocomposite |
| AMCs | Aluminum matrix composites |
| ARB | Accumulative roll bonding |
| ASTM | American society for testing and materials |
| ASTM E8/E8M | Standard test method for tension testing on metallic materials |
| CS | Centrifugal casting |
| EG | Exfoliated graphite |
| FDM | Fused deposition modeling |
| FE | Finite element |
| FTIR | Fourier transform infrared |
| GNP | Graphene nanoparticles |
| GPI | Gas pressure infiltration |
| HEBMMS | High energy ball mill mixing & sintering |
| HAMCs | Hybrid aluminum matrix composites |
| HPCT | High pressure centrifugal infiltration |
| MI | Melt infiltration |
| MMCs | Metal-matrix nanocomposites |
| MS | Microwave sintering |
| NC | Nanocomposites |
| RVE | Representative volumetric element |
| PI | Pressure infiltration |
| SD | Spray deposition |
| SE | Screw extrusion |
| SEM | Scanning electronic microscope |
| SPS | Spark plasma sintering |
| VGS | Vacuum/gas sintering |
| VI | Vapour infiltration |
| VPI | Vacuum pressure infiltration |

## Author contributions

Ayat Bozeya: conceptualization, methodology, supervision, writing – reviewing and editing, project administration, validation, resources. Hasan Bawa'neh: software, formal analysis, writing – original draft. Bashar Lababneh: visualization, investigation, methodology. Ahmad Malkawi: writing – original draft, investigation, methodology.

## Data availability

Data for this article are available at project (**https://justedujo-my.sharepoint.com/:f:/g/personal/aabouzieh_just_edu_jo/EqSrJc36U7lOuM2RsRFXincBMFAu4aoHeCc7Gg8s8qeFQg?e=xxFYnE**).

## Conflicts of interest

The authors declare that they have no known competing financial interests or personal relationships that could have appeared to influence the work reported in this paper.

## Acknowledgements

The authors would like to acknowledge Eng. Rawan Hayajneh, Eng. Deema Al Shorman from institute of nanotechnology at Jordan University of Science and Technology (JUST) for their help in characterizing the samples, and the institute of Nanotechnology at JUST for hosting the research project.

## References

1 L. Mohammed, M. N. M. Ansari, G. Pua, M. Jawaid and M. S. Islam, *Int. J. Polym. Sci.*, 2015, 243947, DOI: **10.1155/2015/243947**.
2 ed. M. Di Ventra, S. Evoy and J. R. Heflin, *Introduction to Nanoscale Science and Technology*, Springer, New York, NY, 1st edn, 2004, DOI: **10.1007/b119185**.
3 P. H. C. Camargo, K. G. Satyanarayana and F. Wypych, *Mater. Res.*, 2009, **12**(1), 1–39.
4 T. Sathishkumar, J. Naveen and S. Satheeshkumar, *J. Reinf. Plast. Compos.*, 2014, **33**(5), 454–471, DOI: **10.1177/0731684413516393**.
5 C. S. M. F. Costa, A. C. Fonseca, A. C. Serra and J. F. J. Coelho, *Polym. Rev.*, 2016, **56**(2), 362–383, DOI: **10.1080/15583724.2015.1108334**.
6 S. H. Din, M. A. Shah, N. A. Sheikh and M. M. Butt, *Charact. Appl. Nanomater.*, 2019, 2, DOI: **10.24294/can.v2i1.875**.
7 S. Pina, J. M. Oliveira and R. L. Reis, *Adv. Mater.*, 2015, **27**(7), 1143–1169.
8 M. A. Rafiee, J. Rafiee, Z. Wang, H. Song, Z.-Z. Yu and N. Koratkar, *ACS Nano*, 2009, **3**(12), 3884–3890.
9 M. Mariano, N. El Kissi and A. Dufresne, *J. Polym. Sci., Part B: Polym. Phys.*, 2014, **52**(12), 791–806, DOI: **10.1002/polb.23490**.
10 P. M. Ajayan, in *Nanocomposite science and technology*, ed. P. M. Ajayan, L. S. chadler and P. V. Braun, Wiley-VCH Verlag GmbH & Co. KGaA, 2003, pp. 1–76, DOI: **10.1002/3527602127.ch1**.
11 H. P. S. Abdul Khalil, R. Dungani, M. S. Hossain, N. L. M. Suraya, S. Aprilia, A. A. Astimar, Z. Nahrul Hayawin and Y. Davoudpour, 15 - Mechanical properties of oil palm biocomposites enhanced with micro to nano-biofillers, in *Biocomposites*, ed. M. Misra, J. K. Pandey and A. K. Mohanty, Woodhead Publishing Series in Composites Science and Engineering, Woodhead Publishing, 2015, pp. 401–435.
12 J. Goni, I. Mitxelena and J. Coleto, *Mater. Sci. Technol.*, 2000, **16**(7–8), 743–746.
13 M. Patel, M. K. Singh and A. K. Sahu, in *Innovative Product Design and Intelligent Manufacturing Systems*, ed. B. Deepak, D. Parhi and P. Jena, Lecture Notes in Mechanical Engineering, Springer, Singapore, 2020, DOI: **10.1007/978-981-15-2696-1_35**.
14 J. Rino, D. Chandramohan and K. S. Sucitharan, *Int. J. Sci. Res.*, 2012, **1**(3), 196–302.
15 T. Mahmoudi, Y. Wang and Y.-B. Hahn, *Nano Energy*, 2018, **47**, 51–56, DOI: **10.1016/j.nanoen.2018.02.047**.
16 S. Stankovich, D. A. Dikin, G. H. B. Dommett, K. M. Kohlhaas, E. J. Zimney, E. A. Stach, R. D. Piner, S. T. Naguyen and R. S. Ruoff, *Nature*, 2006, **442**, 282–286, DOI: **10.1038/nature04969**.
17 V. B. Mohan, K. Lau, D. Hui and D. Bhattacharyya, *Composites, Part B*, 2018, **142**, 200–220.
18 S. Park and R. S. Ruoff, *Nat. Nanotechnol.*, 2009, **4**, 217–224, DOI: **10.1038/nnano.2009.58**.
19 F. Wang, L. T. Drzal, Y. Qin and Z. Huang, *J. Mater. Sci.*, 2015, **50**(3), 1082–1093.
20 S. N. Monteiro, V. Calado, R. J. S. Rodriguez and F. M. Margem, *Mater. Sci. Eng., A*, 2012, **557**, 17–28.
21 J. Liang, Y. Xu, Y. Huang, L. Zhang, Y. Wang, Y. Ma, F. Li, T. Guo and Y. Chen, *J. Phys. Chem. C*, 2009, **113**, 9921–9927.
22 K. Müller, E. Bugnicourt, M. Latorre, M. Jorda, Y. Echegoyen Sanz, J. M. Lagaron, O. Miesbauer, A. Bianchin, S. Hankin and U. Bölz, *Nanomaterials*, 2017, **7**, 74.
23 M. K. Uddin, *Chem. Eng. J.*, 2017, **308**, 438–462.
24 I. Savic, S. Stojiljkovic, I. Savic and D. Gajic, In *Clays and Clay Minerals: Geological Origin, Mechanical Properties and Industrial Applications*, ed. L. R. Wesley, Nova Science Publishers, New York, NY, USA, 2014, pp. 379–402.
25 S. Matei, M. Stoicanescu, V. Bela, E. Tiron and A. Crisan, *Adv. Mech. Eng.*, 2021, **13**(4), DOI: **10.1177/16878140211011888**.
26 Metals Handbook, Properties and Selection: Nonferrous Alloys and Special-Purpose Materials, ASM International, 10th edn, 1990, vol. 2.
27 Y. Sun, *Structures*, 2023, **57**, 105290, DOI: **10.1016/j.istruc.2023.105290**.
28 E. W. A. Fanani, E. Surojo, A. R. Prabowo and H. I. Akbar, *Metals*, 2021, **11**, 1919, DOI: **10.3390/met11121919**.
29 A. B. Mapossa, A. H. da Silva Júnior, C. R. S. de Oliveira and W. Mhike, *Polymers*, 2023, **15**, 3443, DOI: **10.3390/polym15163443**.
30 M. Ravi Shankar, S. Chandrasekar, W. D. Compton and A. H. King, *Mater. Sci. Eng. A*, 2005, **410–411**, 364–368, DOI: **10.1016/J.MSEA.2005.08.137**.
31 S. Das, M. Chandrasekaran and S. Samanta, *Mater. Today Proc.*, 2018, **5**(9), 18110–18119, DOI: **10.1016/j.matpr.2018.06.146**.
32 S. Bahl, *Mater. Today Proc.*, 2021, **39**, 317–323.
33 R. Arunachalam, P. K. Krishnan and R. Muraliraja, *J. Manuf. Process.*, 2019, **42**, 213–245, DOI: **10.1016/j.jmapro.2019.04.017**.
34 L. Vertuccio, F. De Santis, R. Pantani, K. Lafdi and L. Guadagno, *Composites, Part B*, 2019, **162**, 600–610, DOI: **10.1016/j.compositesb.2019.01.045**.

35 M. Aziz, F. Syuhada and J. Jaafar, *J. Teknol.*, 2014, **69**(9), 11–14.
36 T. Ravindra Reddy, S. Kaneko, T. Endo and S. Lakshmi Reddy, *J. Laser Opt. Photonics*, 2017, **4**, 171, DOI: **10.4172/2469-410X.1000171**.
37 H. Yin, W. Zhang, L. Zhu, F. Meng, J. Liu and G. Wen, *Compos. Struct.*, 2022, **304**(1), 116397, DOI: **10.1016/j.compstruct.2022.116397**.
38 P. Samal and P. R. Vundavilli, *IOP Conf. Ser.:Mater. Sci. Eng.*, 2019, **653**, 012047, DOI: **10.1088/1757-899X/653/1/012047**.
39 X. Du, K. Zheng and F. Liu, *Mater. Technol.*, 2018, **52**(6), 763–768, DOI: **10.17222/mit.2018.021**.
40 W. D. Callister Jr and D. G. Rethwisch. *Materials science and engineering: an introduction*, John Wiley & Sons, 2020.
41 M. Dahiya, V. Khanna and S. A. Bansal, *Carbon Lett.*, 2023, **33**, 1601–1613, DOI: **10.1007/s42823-023-00543-x**.